

Study of dipion bottomonium transitions and search for the $h_b(1P)$ state

J. P. Lees,¹ V. Poireau,¹ V. Tisserand,¹ J. Garra Tico,² E. Grauges,² M. Martinelli,^{3a,3b} D. A. Milanese,^{3a} A. Palano,^{3a,3b} M. Pappagallo,^{3a,3b} G. Eigen,⁴ B. Stugu,⁴ L. Sun,⁴ D. N. Brown,⁵ L. T. Kerth,⁵ Yu. G. Kolomensky,⁵ G. Lynch,⁵ H. Koch,⁶ T. Schroeder,⁶ D. J. Asgeirsson,⁷ C. Hearty,⁷ T. S. Mattison,⁷ J. A. McKenna,⁷ A. Khan,⁸ V. E. Blinov,⁹ A. R. Buzykaev,⁹ V. P. Druzhinin,⁹ V. B. Golubev,⁹ E. A. Kravchenko,⁹ A. P. Onuchin,⁹ S. I. Serednyakov,⁹ Yu. I. Skovpen,⁹ E. P. Solodov,⁹ K. Yu. Todyshev,⁹ A. N. Yushkov,⁹ M. Bondioli,¹⁰ S. Curry,¹⁰ D. Kirkby,¹⁰ A. J. Lankford,¹⁰ M. Mandelkern,¹⁰ D. P. Stoker,¹⁰ H. Atmacan,¹¹ J. W. Gary,¹¹ F. Liu,¹¹ O. Long,¹¹ G. M. Vitug,¹¹ C. Campagnari,¹² T. M. Hong,¹² D. Kovalskyi,¹² J. D. Richman,¹² C. A. West,¹² A. M. Eisner,¹³ J. Kroseberg,¹³ W. S. Lockman,¹³ A. J. Martinez,¹³ T. Schalk,¹³ B. A. Schumm,¹³ A. Seiden,¹³ C. H. Cheng,¹⁴ D. A. Doll,¹⁴ B. Echenard,¹⁴ K. T. Flood,¹⁴ D. G. Hitlin,¹⁴ P. Ongmongkolkul,¹⁴ F. C. Porter,¹⁴ A. Y. Rakitin,¹⁴ R. Andreassen,¹⁵ M. S. Dubrovin,¹⁵ B. T. Meadows,¹⁵ M. D. Sokoloff,¹⁵ P. C. Bloom,¹⁶ W. T. Ford,¹⁶ A. Gaz,¹⁶ M. Nagel,¹⁶ U. Nauenberg,¹⁶ J. G. Smith,¹⁶ S. R. Wagner,¹⁶ R. Ayad,^{17,*} W. H. Toki,¹⁷ B. Spaan,¹⁸ M. J. Kobel,¹⁹ K. R. Schubert,¹⁹ R. Schwierz,¹⁹ D. Bernard,²⁰ M. Verderi,²⁰ P. J. Clark,²¹ S. Playfer,²¹ D. Bettoni,^{22a} C. Bozzi,^{22a} R. Calabrese,^{22a,22b} G. Cibinetto,^{22a,22b} E. Fioravanti,^{22a,22b} I. Garzia,^{22a,22b} E. Luppi,^{22a,22b} M. Menerato,^{22a,22b} M. Negrini,^{22a,22b} L. Piemontese,^{22a} R. Baldini-Ferrolì,²³ A. Calcaterra,²³ R. de Sangro,²³ G. Finocchiaro,²³ M. Nicolaci,²³ P. Patteri,²³ I. M. Peruzzi,^{23,†} M. Piccolo,²³ M. Rama,²³ A. Zallo,²³ R. Contri,^{24a,24b} E. Guido,^{24a,24b} M. Lo Vetere,^{24a,24b} M. R. Monge,^{24a,24b} S. Passaggio,^{24a} C. Patrignani,^{24a,24b} E. Robutti,^{24a} B. Bhuyan,²⁵ V. Prasad,²⁵ C. L. Lee,²⁶ M. Morii,²⁶ A. J. Edwards,²⁷ A. Adametz,²⁸ J. Marks,²⁸ U. Uwer,²⁸ F. U. Bernlochner,²⁹ M. Ebert,²⁹ H. M. Lacker,²⁹ T. Lueck,²⁹ P. D. Dauncey,³⁰ M. Tibbetts,³⁰ P. K. Behera,³¹ U. Mallik,³¹ C. Chen,³² J. Cochran,³² H. B. Crawley,³² W. T. Meyer,³² S. Prell,³² E. I. Rosenberg,³² A. E. Rubin,³² A. V. Gritsan,³³ Z. J. Guo,³³ N. Arnaud,³⁴ M. Davier,³⁴ G. Grosdidier,³⁴ F. Le Diberder,³⁴ A. M. Lutz,³⁴ B. Malaescu,³⁴ P. Roudeau,³⁴ M. H. Schune,³⁴ A. Stocchi,³⁴ G. Wormser,³⁴ D. J. Lange,³⁵ D. M. Wright,³⁵ I. Bingham,³⁶ C. A. Chavez,³⁶ J. P. Coleman,³⁶ J. R. Fry,³⁶ E. Gabathuler,³⁶ D. E. Hutchcroft,³⁶ D. J. Payne,³⁶ C. Touramanis,³⁶ A. J. Bevan,³⁷ F. Di Lodovico,³⁷ R. Sacco,³⁷ M. Sigamani,³⁷ G. Cowan,³⁸ S. Paramesvaran,³⁸ D. N. Brown,³⁹ C. L. Davis,³⁹ A. G. Denig,⁴⁰ M. Fritsch,⁴⁰ W. Gradl,⁴⁰ A. Hafner,⁴⁰ E. Prencipe,⁴⁰ K. E. Alwyn,⁴¹ D. Bailey,⁴¹ R. J. Barlow,⁴¹ G. Jackson,⁴¹ G. D. Lafferty,⁴¹ R. Cenci,⁴² B. Hamilton,⁴² A. Jawahery,⁴² D. A. Roberts,⁴² G. Simi,⁴² C. Dallapiccola,⁴³ R. Cowan,⁴⁴ D. Dujmic,⁴⁴ G. Sciolla,⁴⁴ D. Lindemann,⁴⁵ P. M. Patel,⁴⁵ S. H. Robertson,⁴⁵ M. Schram,⁴⁵ P. Biassoni,^{46a,46b} A. Lazzaro,^{46a,46b} V. Lombardo,^{46a} F. Palombo,^{46a,46b} S. Stracka,^{46a,46b} L. Cremaldi,⁴⁷ R. Godang,^{47,‡} R. Kroeger,⁴⁷ P. Sonnek,⁴⁷ D. J. Summers,⁴⁷ X. Nguyen,⁴⁸ P. Taras,⁴⁸ G. De Nardo,^{49a,49b} D. Monorchio,^{49a,49b} G. Onorato,^{49a,49b} C. Sciacca,^{49a,49b} G. Raven,⁵⁰ H. L. Snoek,⁵⁰ C. P. Jessop,⁵¹ K. J. Knoepfel,⁵¹ J. M. LoSecco,⁵¹ W. F. Wang,⁵¹ K. Honscheid,⁵² R. Kass,⁵² J. Brau,⁵³ R. Frey,⁵³ N. B. Sinev,⁵³ D. Strom,⁵³ E. Torrence,⁵³ E. Feltresi,^{54a,54b} N. Gagliardi,^{54a,54b} M. Margoni,^{54a,54b} M. Morandin,^{54a} M. Posocco,^{54a} M. Rotondo,^{54a} F. Simonetto,^{54a,54b} R. Stroili,^{54a,54b} E. Ben-Haim,⁵⁵ M. Bomben,⁵⁵ G. R. Bonneaud,⁵⁵ H. Briand,⁵⁵ G. Calderini,⁵⁵ J. Chauveau,⁵⁵ O. Hamon,⁵⁵ Ph. Leruste,⁵⁵ G. Marchiori,⁵⁵ J. Ocariz,⁵⁵ S. Sitt,⁵⁵ M. Biasini,^{56a,56b} E. Manoni,^{56a,56b} S. Pacetti,^{56a,56b} A. Rossi,^{56a,56b} C. Angelini,^{57a,57b} G. Batignani,^{57a,57b} S. Bettarini,^{57a,57b} M. Carpinelli,^{57a,57b,§} G. Casarosa,^{57a,57b} A. Cervelli,^{57a,57b} F. Forti,^{57a,57b} M. A. Giorgi,^{57a,57b} A. Lusiani,^{57a,57c} N. Neri,^{57a,57b} B. Oberhof,^{57a,57b} E. Paoloni,^{57a,57b} A. Perez,^{57a} G. Rizzo,^{57a,57b} J. J. Walsh,^{57a} D. Lopes Pegna,⁵⁸ C. Lu,⁵⁸ J. Olsen,⁵⁸ A. J. S. Smith,⁵⁸ A. V. Telnov,⁵⁸ F. Anulli,^{59a} G. Cavoto,^{59a} R. Faccini,^{59a,59b} F. Ferrarotto,^{59a} F. Ferroni,^{59a,59b} M. Gaspero,^{59a,59b} L. Li Gioi,^{59a} M. A. Mazzoni,^{59a} G. Piredda,^{59a} C. Büniger,⁶⁰ O. Grünberg,⁶⁰ T. Hartmann,⁶⁰ T. Leddig,⁶⁰ H. Schröder,⁶⁰ R. Waldi,⁶⁰ T. Adye,⁶¹ E. O. Olaiya,⁶¹ F. F. Wilson,⁶¹ S. Emery,⁶² G. Hamel de Monchenault,⁶² G. Vasseur,⁶² Ch. Yèche,⁶² D. Aston,⁶³ D. J. Bard,⁶³ R. Bartoldus,⁶³ J. F. Benitez,⁶³ C. Cartaro,⁶³ M. R. Convery,⁶³ J. Dorfan,⁶³ G. P. Dubois-Felsmann,⁶³ W. Dunwoodie,⁶³ R. C. Field,⁶³ M. Franco Sevilla,⁶³ B. G. Fulsom,⁶³ A. M. Gabareen,⁶³ M. T. Graham,⁶³ P. Grenier,⁶³ C. Hast,⁶³ W. R. Innes,⁶³ M. H. Kelsey,⁶³ H. Kim,⁶³ P. Kim,⁶³ M. L. Kocian,⁶³ D. W. G. S. Leith,⁶³ P. Lewis,⁶³ S. Li,⁶³ B. Lindquist,⁶³ S. Luitz,⁶³ V. Luth,⁶³ H. L. Lynch,⁶³ D. B. MacFarlane,⁶³ D. R. Muller,⁶³ H. Neal,⁶³ S. Nelson,⁶³ I. Ofte,⁶³ M. Perl,⁶³ T. Pulliam,⁶³ B. N. Ratcliff,⁶³ A. Roodman,⁶³ A. A. Salnikov,⁶³ V. Santoro,⁶³ R. H. Schindler,⁶³ A. Snyder,⁶³ D. Su,⁶³ M. K. Sullivan,⁶³ J. Va'vra,⁶³ A. P. Wagner,⁶³ M. Weaver,⁶³ W. J. Wisniewski,⁶³ M. Wittgen,⁶³ D. H. Wright,⁶³ H. W. Wulsin,⁶³ A. K. Yarritu,⁶³ C. C. Young,⁶³ V. Ziegler,⁶³ W. Park,⁶⁴ M. V. Purohit,⁶⁴ R. M. White,⁶⁴ J. R. Wilson,⁶⁴ A. Randle-Conde,⁶⁵ S. J. Sekula,⁶⁵ M. Bellis,⁶⁶ P. R. Burchat,⁶⁶ T. S. Miyashita,⁶⁶ M. S. Alam,⁶⁷ J. A. Ernst,⁶⁷ R. Gorodeisky,⁶⁸ N. Guttman,⁶⁸ D. R. Peimer,⁶⁸ A. Soffer,⁶⁸ P. Lund,⁶⁹ S. M. Spanier,⁶⁹ R. Eckmann,⁷⁰ J. L. Ritchie,⁷⁰ A. M. Ruland,⁷⁰ C. J. Schilling,⁷⁰ R. F. Schwitters,⁷⁰ B. C. Wray,⁷⁰ J. M. Izen,⁷¹ X. C. Lou,⁷¹ F. Bianchi,^{72a,72b} D. Gamba,^{72a,72b}

L. Lanceri,^{73a,73b} L. Vitale,^{73a,73b} N. Lopez-March,⁷⁴ F. Martinez-Vidal,⁷⁴ A. Oyanguren,⁷⁴ H. Ahmed,⁷⁵
 J. Albert,⁷⁵ Sw. Banerjee,⁷⁵ H. H. F. Choi,⁷⁵ G. J. King,⁷⁵ R. Kowalewski,⁷⁵ M. J. Lewczuk,⁷⁵ C. Lindsay,⁷⁵
 I. M. Nugent,⁷⁵ J. M. Roney,⁷⁵ R. J. Sobie,⁷⁵ T. J. Gershon,⁷⁶ P. F. Harrison,⁷⁶ T. E. Latham,⁷⁶ E. M. T. Puccio,⁷⁶
 H. R. Band,⁷⁷ S. Dasu,⁷⁷ Y. Pan,⁷⁷ R. Prepost,⁷⁷ C. O. Vuosalo,⁷⁷ and S. L. Wu⁷⁷

(The *BABAR* Collaboration)

- ¹Laboratoire d'Annecy-le-Vieux de Physique des Particules (LAPP), Université de Savoie, CNRS/IN2P3, F-74941 Annecy-Le-Vieux, France
- ²Universitat de Barcelona, Facultat de Física, Departament ECM, E-08028 Barcelona, Spain
- ^{3a}INFN Sezione di Bari, I-70126 Bari, Italy
- ^{3b}Dipartimento di Fisica, Università di Bari, I-70126 Bari, Italy
- ⁴University of Bergen, Institute of Physics, N-5007 Bergen, Norway
- ⁵Lawrence Berkeley National Laboratory and University of California, Berkeley, California 94720, USA
- ⁶Ruhr Universität Bochum, Institut für Experimentalphysik 1, D-44780 Bochum, Germany
- ⁷University of British Columbia, Vancouver, British Columbia, Canada V6T 1Z1
- ⁸Brunel University, Uxbridge, Middlesex UB8 3PH, United Kingdom
- ⁹Budker Institute of Nuclear Physics, Novosibirsk 630090, Russia
- ¹⁰University of California at Irvine, Irvine, California 92697, USA
- ¹¹University of California at Riverside, Riverside, California 92521, USA
- ¹²University of California at Santa Barbara, Santa Barbara, California 93106, USA
- ¹³University of California at Santa Cruz, Institute for Particle Physics, Santa Cruz, California 95064, USA
- ¹⁴California Institute of Technology, Pasadena, California 91125, USA
- ¹⁵University of Cincinnati, Cincinnati, Ohio 45221, USA
- ¹⁶University of Colorado, Boulder, Colorado 80309, USA
- ¹⁷Colorado State University, Fort Collins, Colorado 80523, USA
- ¹⁸Technische Universität Dortmund, Fakultät Physik, D-44221 Dortmund, Germany
- ¹⁹Technische Universität Dresden, Institut für Kern- und Teilchenphysik, D-01062 Dresden, Germany
- ²⁰Laboratoire Leprince-Ringuet, Ecole Polytechnique, CNRS/IN2P3, F-91128 Palaiseau, France
- ²¹University of Edinburgh, Edinburgh EH9 3JZ, United Kingdom
- ^{22a}INFN Sezione di Ferrara, I-44100 Ferrara, Italy;
- ^{22b}Dipartimento di Fisica, Università di Ferrara, I-44100 Ferrara, Italy
- ²³INFN Laboratori Nazionali di Frascati, I-00044 Frascati, Italy
- ^{24a}INFN Sezione di Genova, I-16146 Genova, Italy;
- ^{24b}Dipartimento di Fisica, Università di Genova, I-16146 Genova, Italy
- ²⁵Indian Institute of Technology Guwahati, Guwahati, Assam, 781 039, India
- ²⁶Harvard University, Cambridge, Massachusetts 02138, USA
- ²⁷Harvey Mudd College, Claremont, California 91711, USA
- ²⁸Universität Heidelberg, Physikalisches Institut, Philosophenweg 12, D-69120 Heidelberg, Germany
- ²⁹Humboldt-Universität zu Berlin, Institut für Physik, Newtonstraße 15, D-12489 Berlin, Germany
- ³⁰Imperial College London, London, SW7 2AZ, United Kingdom
- ³¹University of Iowa, Iowa City, Iowa 52242, USA
- ³²Iowa State University, Ames, Iowa 50011-3160, USA
- ³³Johns Hopkins University, Baltimore, Maryland 21218, USA
- ³⁴Laboratoire de l'Accélérateur Linéaire, IN2P3/CNRS et Université Paris-Sud 11, Centre Scientifique d'Orsay, Boite Postale 34, F-91898 Orsay Cedex, France
- ³⁵Lawrence Livermore National Laboratory, Livermore, California 94550, USA
- ³⁶University of Liverpool, Liverpool L69 7ZE, United Kingdom
- ³⁷Queen Mary, University of London, London, E1 4NS, United Kingdom
- ³⁸University of London, Royal Holloway and Bedford New College, Egham, Surrey TW20 0EX, United Kingdom
- ³⁹University of Louisville, Louisville, Kentucky 40292, USA
- ⁴⁰Johannes Gutenberg-Universität Mainz, Institut für Kernphysik, D-55099 Mainz, Germany
- ⁴¹University of Manchester, Manchester M13 9PL, United Kingdom
- ⁴²University of Maryland, College Park, Maryland 20742, USA
- ⁴³University of Massachusetts, Amherst, Massachusetts 01003, USA

- ⁴⁴*Massachusetts Institute of Technology, Laboratory for Nuclear Science, Cambridge, Massachusetts 02139, USA*
- ⁴⁵*McGill University, Montréal, Québec, Canada H3A 2T8*
- ^{46a}*INFN Sezione di Milano I-20133 Milano, Italy;*
- ^{46b}*Dipartimento di Fisica, Università di Milano, I-20133 Milano, Italy*
- ⁴⁷*University of Mississippi, University, Mississippi 38677, USA*
- ⁴⁸*Université de Montréal, Physique des Particules, Montréal, Québec, Canada H3C 3J7*
- ^{49a}*INFN Sezione di Napoli, I-80126 Napoli, Italy;*
- ^{49b}*Dipartimento di Scienze Fisiche, Università di Napoli Federico II, I-80126 Napoli, Italy*
- ⁵⁰*NIKHEF, National Institute for Nuclear Physics and High Energy Physics, NL-1009 DB Amsterdam, The Netherlands*
- ⁵¹*University of Notre Dame, Notre Dame, Indiana 46556, USA*
- ⁵²*Ohio State University, Columbus, Ohio 43210, USA*
- ⁵³*University of Oregon, Eugene, Oregon 97403, USA*
- ^{54a}*INFN Sezione di Padova, I-35131 Padova, Italy;*
- ^{54b}*Dipartimento di Fisica, Università di Padova, I-35131 Padova, Italy*
- ⁵⁵*Laboratoire de Physique Nucléaire et de Hautes Energies, IN2P3/CNRS, Université Pierre et Marie Curie-Paris6, Université Denis Diderot-Paris7, F-75252 Paris, France*
- ^{56a}*INFN Sezione di Perugia. I-06100 Perugia, Italy;*
- ^{56b}*Dipartimento di Fisica, Università di Perugia, I-06100 Perugia, Italy*
- ^{57a}*INFN Sezione di Pisa, I-56127 Pisa, Italy;*
- ^{57b}*Dipartimento di Fisica, Università di Pisa, I-56127 Pisa, Italy;*
- ^{57c}*Scuola Normale Superiore di Pisa, I-56127 Pisa, Italy*
- ⁵⁸*Princeton University, Princeton, New Jersey 08544, USA*
- ^{59a}*INFN Sezione di Roma, I-00185 Roma, Italy;*
- ^{59b}*Dipartimento di Fisica, Università di Roma La Sapienza, I-00185 Roma, Italy*
- ⁶⁰*Universität Rostock, D-18051 Rostock, Germany*
- ⁶¹*Rutherford Appleton Laboratory, Chilton, Didcot, Oxon, OX11 0QX, United Kingdom*
- ⁶²*CEA, Irfu, SPP, Centre de Saclay, F-91191 Gif-sur-Yvette, France*
- ⁶³*SLAC National Accelerator Laboratory, Stanford, California 94309 USA*
- ⁶⁴*University of South Carolina, Columbia, South Carolina 29208, USA*
- ⁶⁵*Southern Methodist University, Dallas, Texas 75275, USA*
- ⁶⁶*Stanford University, Stanford, California 94305-4060, USA*
- ⁶⁷*State University of New York, Albany, New York 12222, USA*
- ⁶⁸*Tel Aviv University, School of Physics and Astronomy, Tel Aviv, 69978, Israel*
- ⁶⁹*University of Tennessee, Knoxville, Tennessee 37996, USA*
- ⁷⁰*University of Texas at Austin, Austin, Texas 78712, USA*
- ⁷¹*University of Texas at Dallas, Richardson, Texas 75083, USA*
- ^{72a}*INFN Sezione di Torino, I-10125 Torino, Italy;*
- ^{72b}*Dipartimento di Fisica Sperimentale, Università di Torino, I-10125 Torino, Italy*
- ^{73a}*INFN Sezione di Trieste, I-34127 Trieste, Italy;*
- ^{73b}*Dipartimento di Fisica, Università di Trieste, I-34127 Trieste, Italy*
- ⁷⁴*IFIC, Universitat de Valencia-CSIC, E-46071 Valencia, Spain*
- ⁷⁵*University of Victoria, Victoria, British Columbia, Canada V8W 3P6*
- ⁷⁶*Department of Physics, University of Warwick, Coventry CV4 7AL, United Kingdom*
- ⁷⁷*University of Wisconsin, Madison, Wisconsin 53706, USA*

(Received 24 May 2011; published 27 July 2011)

We study inclusive dipion decays using a sample of $108 \times 10^6 Y(3S)$ events recorded with the BABAR detector. We search for the decay mode $Y(3S) \rightarrow \pi^+ \pi^- h_b(1P)$ and find no evidence for the bottomonium spin-singlet state $h_b(1P)$ in the invariant mass distribution recoiling against the $\pi^+ \pi^-$ system. Assuming the $h_b(1P)$ mass to be $9.900 \text{ GeV}/c^2$, we measure the upper limit on the branching fraction $\mathcal{B}[Y(3S) \rightarrow \pi^+ \pi^- h_b(1P)] < 1.2 \times 10^{-4}$, at 90% confidence level. We also investigate the $\chi_{bJ}(2P) \rightarrow \pi^+ \pi^- \chi_{bJ}(1P)$, $Y(3S) \rightarrow \pi^+ \pi^- Y(2S)$, and $Y(2S) \rightarrow \pi^+ \pi^- Y(1S)$ dipion transitions and

*Now at Temple University, Philadelphia, PA 19122, USA.

†Also with Università di Perugia, Dipartimento di Fisica, Perugia, Italy.

‡Now at University of South Alabama, Mobile, AL 36688, USA.

§Also with Università di Sassari, Sassari, Italy.

present an improved measurement of the branching fraction of the $Y(3S) \rightarrow \pi^+ \pi^- Y(2S)$ decay and of the $Y(3S) - Y(2S)$ mass difference.

DOI: 10.1103/PhysRevD.84.011104

PACS numbers: 13.20.Gd, 14.40.Pq, 14.65.Fy

Studies of $b\bar{b}$ (*bottomonium*) and $c\bar{c}$ (*charmonium*) bound states provide insight about interquark forces. The measurement of the hyperfine mass splitting between triplet and singlet states in quarkonium systems discriminates between various models and tests lattice QCD and potential nonrelativistic QCD calculations [1]. Observation of the P -wave singlet ground state of charmonium, $h_c(1P)$, was recently confirmed and its mass precisely measured, yielding the hyperfine splitting for the charmonium $1P$ states $\Delta M_{hf}(1P)_{c\bar{c}} \equiv \langle M(^3P_J) \rangle_{c\bar{c}} - M(^1P_1)_{c\bar{c}} = +0.08 \pm 0.18(\text{stat.}) \pm 0.12(\text{syst.}) \text{ MeV}/c^2$ [2], where $\langle M(^3P_J) \rangle$ is the spin-weighted average mass of the $J = 0, 1, 2$ ground states. The hyperfine splitting $\Delta M_{hf}(1P)_{b\bar{b}} \equiv \langle M(^3P_J) \rangle_{b\bar{b}} - M(^1P_1)_{b\bar{b}}$ for bottomonium states is expected to be no more than a few MeV/c^2 [3]. The 3P_J $b\bar{b}$ ground states are well established, and their spin-weighted mass average is $\langle M(^3P_J)_{b\bar{b}} \rangle = [M(\chi_{b0}(1P)) + 3M(\chi_{b1}(1P)) + 5M(\chi_{b2}(1P))]/9 = 9.89987 \pm 0.00027 \text{ GeV}/c^2$ [4]. The $h_b(1P)$, hereafter referred to as the h_b , is expected to decay predominantly to ggg (57% branching fraction), $\gamma\eta_b$ (41%), and $gg\gamma$ (2%), and its width is predicted to be of order 0.1 MeV [5].

We report, herein, a search for the h_b through the hadronic transition $Y(3S) \rightarrow \pi^+ \pi^- h_b(1P)$. The CLEO Collaboration searched for the h_b in the reactions $Y(3S) \rightarrow \pi^0 h_b$ and $Y(3S) \rightarrow \pi^+ \pi^- h_b$, setting upper limits at 90% confidence level (CL) for the branching fractions $\mathcal{B}[Y(3S) \rightarrow \pi^0 h_b] < 2.7 \times 10^{-3}$ and $\mathcal{B}_Y \equiv \mathcal{B}[Y(3S) \rightarrow \pi^+ \pi^- h_b] < 1.8 \times 10^{-3}$, assuming the h_b mass $m(h_b)$ to be 9.900 GeV/c^2 [6]. The BABAR Collaboration recently reported evidence for the h_b in $Y(3S) \rightarrow \pi^0 h_b$, $h_b \rightarrow \eta_b \gamma$ decays [7]. Preliminary results of a search for the h_b in the reaction $e^+ e^- \rightarrow \pi^+ \pi^- h_b$, reporting the observation of the h_b meson, have been announced by the Belle Collaboration [8]. Theoretical predictions for \mathcal{B}_Y span 1 order of magnitude. References [9–11] predict a branching fraction between 2.2×10^{-4} and 8.0×10^{-4} , while Ref. [12] predicts a rate of 10^{-4} or smaller.

The data sample used in this study was collected with the BABAR detector [13] at the PEP-II asymmetric-energy $e^+ e^-$ storage rings at the SLAC National Accelerator Laboratory. It consists of 25.6 fb^{-1} of integrated luminosity collected at a $e^+ e^-$ center-of-mass (c.m.) energy of 10.355 GeV, corresponding to the mass of the $Y(3S)$ resonance. The number of recorded $Y(3S)$ events is 108×10^6 . An additional sample of 2.5 fb^{-1} recorded at the $Y(3S)$ energy (“10%” sample) and a 2.6 fb^{-1} sample collected 30 MeV below the $Y(3S)$ resonance (“off-peak” sample) are used for background and calibration studies.

The momenta of charged particles are reconstructed using a combination of a five-layer double-sided silicon-strip detector and a 40-layer drift chamber, both operating in the 1.5-T magnetic field of a superconducting solenoid. Photons are detected using a CsI(Tl) electromagnetic calorimeter, which is also inside the magnet coil. Charged hadron identification is achieved through measurements of particle energy loss in the tracking system and the Cherenkov angle obtained from a detector of internally reflected Cherenkov light.

The $\pi^+ \pi^-$ pairs are selected from oppositely charged tracks that originate from the $e^+ e^-$ interaction region in hadronic events, hence excluding tracks arising from a photon conversion or the decay of a long-lived particle. We search for an h_b signal using a fit to the spectrum of the mass m_R recoiling against the $\pi^+ \pi^-$ system, defined by

$$m_R^2 = (M_{Y(3S)} - E_{\pi\pi}^*)^2 - |\mathbf{P}_{\pi\pi}^*|^2, \quad (1)$$

where $E_{\pi\pi}^*$ and $\mathbf{P}_{\pi\pi}^*$ are, respectively, the measured $\pi\pi$ energy and momentum in the c.m. frame.

The h_b signal is expected to appear as a peak in the m_R distribution on top of a smooth nonpeaking background from continuum events ($e^+ e^- \rightarrow q\bar{q}$ with $q = u, d, s, c$) and bottomonium decays. Several other processes produce peaks in the recoil mass spectrum close to the signal region. Hadronic transitions $Y(3S) \rightarrow \pi^+ \pi^- Y(2S)$ (hereafter denoted $Y^{3 \rightarrow 2}$) produce a peak centered at the $Y(2S)$ mass $m[Y(2S)] = 10.02326 \pm 0.00031 \text{ GeV}/c^2$ [4]. The cascade process $Y(3S) \rightarrow Y(2S)X$, $Y(2S) \rightarrow \pi^+ \pi^- Y(1S)(Y^{2 \rightarrow 1})$ results in a peak centered at 9.791 GeV/c^2 . The peak is offset from the $Y(1S)$ mass by approximately the $Y(3S)$ to $Y(2S)$ mass difference. Doppler shift and broadening further affect the position and width of this peak. When the $Y(2S)$ parent in $Y^{2 \rightarrow 1}$ decays is produced through the $Y^{3 \rightarrow 2}$ channel, a pion from the $Y(3S)$ decay can be combined with an oppositely charged track from the $Y(2S)$ decay to produce a broad distribution centered around 9.9 GeV/c^2 . The $Y(2S)$ is also produced through the initial-state radiation (ISR) process $e^+ e^- \rightarrow \gamma_{\text{ISR}} Y(2S)(Y_{\text{ISR}}^{2 \rightarrow 1})$. Of the nine possible $Y(3S) \rightarrow \chi_{bJ'}(2P)\gamma$, $\chi_{bJ'}(2P) \rightarrow \pi^+ \pi^- \chi_{bJ}(1P)$ decay chains ($\chi_b^{J',J}$) [14], only those for $J' = J = \{1, 2\}$ have been reported [4, 15]; these should generate two narrowly separated peaks near 9.993 GeV/c^2 , while the contributions with $J' \neq J$ or with $J = 0$ are expected to be negligible.

Selection criteria are chosen by optimizing the ratio S/\sqrt{B} between the expected h_b signal yield (S) and the background (B). The signal sample for the optimization is provided by a detailed Monte Carlo (MC) simulation

based on GEANT4 [16], EVTGEN [17], and JETSET [18], while the background sample is obtained from the 10% sample, which is not used for the extraction of the signal. The natural width of the h_b meson, which is predicted to be negligible in comparison with the experimental resolution in m_R (0.009 GeV/ c^2 r.m.s.), is set to zero in the simulation.

Since decays of the h_b via three gluons or to $\eta_b\gamma$ are expected to exhibit a high track multiplicity, we require an event to have between 6 and 16 charged tracks, where the upper restriction reduces contributions due to random combinations of tracks. We further require the ratio of the second to zeroth Fox-Wolfram moment [19] calculated using all charged tracks and unmatched neutral showers in the event to be less than 0.55. The total event energy in the laboratory frame must lie between 6 and 18 GeV, where the lower restriction reduces QED background.

Events must contain two oppositely-charged tracks, each of which is identified as a pion. The pion identification efficiency depends on momentum and polar angle, and is typically about 98%. This requirement provides a rejection factor of order 50 against electrons. The vertex of each reconstructed pion pair must lie within 0.41 cm and be less than $4\sigma_L$ from the nominal interaction point in the transverse plane, where σ_L is the uncertainty evaluated on a candidate-by-candidate basis for the transverse flight length L . We demand the χ^2 probability for the vertex fit to be greater than 0.001.

The phase-space distribution of K_S^0 decays extends up to m_R values of approximately 9.86 GeV/ c^2 and then rapidly decreases. To further suppress the background due to K_S^0 decays, we reject pairs of pions if their vertex is displaced from the nominal interaction point by more than 0.05 cm and $2\sigma_L$ in the transverse plane and if they satisfy $\cos\alpha > 0.95$, where α is the angle between the direction of the dipion candidate momentum and its flight direction in the transverse plane. Candidates removed from the nominal sample that satisfy all other selection criteria constitute a K_S^0 -enriched control sample.

The selected data sample consists of approximately 137×10^6 $\pi^+\pi^-$ candidates in the range $9.750 < m_R < 10.040$ GeV/ c^2 , corresponding to an average of 2.4 selected dipion candidates per event. The fit validation studies described below account for the effect of candidate multiplicity. We evaluate the dipion reconstruction efficiency with MC events, by matching the reconstructed $\pi^+\pi^-$ pairs to the simulated pairs emitted in the bottomonium transition under study on an event-by-event basis. The h_b signal efficiency is $\epsilon = 41.8\%$ for $m(h_b) = 9.900$ GeV/ c^2 , with a $[+6, -3]\%$ variation of ϵ over the $m(h_b)$ range $[9.880, 9.920]$ GeV/ c^2 . A lower reconstruction efficiency of 25.0% (16.7%) is found for the softer $\pi^+\pi^-$ pairs produced in $\chi_b^{J,J}(\Upsilon^{3\rightarrow 2})$ transitions. For the $\Upsilon^{2\rightarrow 1}$ transition, an efficiency of 47.2% is obtained by averaging over the contributions from $X = \gamma\gamma, \pi^0\pi^0$, and $\pi^+\pi^-$.

We perform a χ^2 fit to the m_R spectrum in the range $9.750 < m_R < 10.040$ GeV/ c^2 with a model comprising eight components: nonpeaking background, $\Upsilon^{3\rightarrow 2}, \Upsilon^{2\rightarrow 1}, \Upsilon_{\text{ISR}}^{2\rightarrow 1}, \chi_b^{2,2}, \chi_b^{1,1}, K_S^0 \rightarrow \pi^+\pi^-$, and the h_b signal. The m_R distributions of the signal and background are parametrized using probability density functions (PDFs). We define a two-sided Crystal Ball (TCB) function, which is a Gaussian for $-\alpha_L < (x - x_0)/\sigma < \alpha_R$, and transitions to the power-law tail function $f(x)$ [20]:

$$f(x) = e^{-(1/2)\alpha_i^2} \left(\frac{n_i}{\alpha_i}\right)^{n_i} / \left(\frac{|x - x_0|}{\sigma} + \frac{n_i}{\alpha_i} - \alpha_i\right)^{n_i}, \quad (2)$$

where x_0 and σ are the mean and width of the Gaussian, and the subscript $i = L$ ($i = R$) applies to values $x < x_0$ ($x > x_0$). We model the signal component with a symmetric ($\alpha_L = \alpha_R, n_L = n_R$) TCB shape.

The $\Upsilon^{3\rightarrow 2}$ and $\Upsilon^{2\rightarrow 1}$ peaks are described by sums of an asymmetric TCB shape and an asymmetric Gaussian. Contributions to $\Upsilon^{2\rightarrow 1}$ from $X = \{\pi^+\pi^-, \pi^0\pi^0, \gamma\gamma\}$ are modeled separately because of the different Doppler broadening. Their relative fractions and relative peak positions are fixed according to the world-average values [4] and the MC-simulated m_R spectrum, respectively. For each peak, the ratios of the widths of the TCB and Gaussian functions are fixed to the values found from fitting the corresponding MC spectrum. The PDF of the peaking background from ISR $\Upsilon(2S)$ production is parametrized as a symmetric TCB function whose parameters are determined from simulated events. The yield of $\Upsilon_{\text{ISR}}^{2\rightarrow 1}$ events in the $\Upsilon(3S)$ sample, $[6.6 \pm 1.0(\text{stat.})] \times 10^4$, is determined using the off-peak data. A symmetric TCB function is used as the PDF for both the $\chi_b^{1,1}$ and $\chi_b^{2,2}$ contributions. The peak positions of the $\chi_b^{J,J}$ components relative to the $\Upsilon^{3\rightarrow 2}$ peak are fixed according to the MC simulation. The parameters for the width and tail of the TCB function are common to both $\chi_b^{J,J}$ peaks.

The K_S^0 background is modeled using empirical phase-space functions derived from the MC. Knowledge about the K_S^0 transverse momentum distribution is obtained from fits to the $\pi^+\pi^-$ invariant mass spectrum for the K_S^0 -enriched sample, and is used to correct discrepancies between the data and the MC simulation. The K_S^0 background yield, $(348 \pm 10) \times 10^3$, is obtained from an extrapolation of a fit to the m_R spectrum of the K_S^0 -enriched sample, using a scale factor of 2.5 determined from MC simulation. The nonpeaking background PDF is parametrized by a sixth-order polynomial.

The signal (peaking-background) PDF excludes random combinations of tracks that do not originate from the signal (background) bottomonium transition. Such misreconstructed combinations are included in the nonpeaking term.

To improve fit stability, the fit is performed in two stages: a preliminary fit to fix background parameters

followed by a final fit. The peaking-background PDF parameters and yields are determined from the preliminary, χ^2 -based fit in which the signal component is excluded from the model. The free parameters in the fit are the yields of the continuum background and the peaking-background components $Y^{3\rightarrow 2}$, $Y^{2\rightarrow 1}$, and $\chi_b^{J',J}$; the continuum background PDF parameters; the overall m_R scale of the K_S^0 contribution; the peak positions of the $Y^{3\rightarrow 2}$ and $Y^{2\rightarrow 1}$ components; the overall widths of the PDFs for the $Y^{3\rightarrow 2}$, $Y^{2\rightarrow 1}$, and $\chi_b^{J',J}$ components. The χ^2 per degree of freedom after the preliminary fit is $364/272 \approx 1.3$, where the largest contributions arise from a few isolated bins near 9.79 and 10.02 GeV/c^2 . As the measurement is dominated by systematic uncertainties, we evaluate the χ^2 distribution on simulated pseudoexperiments accounting for the dominant sources of systematic uncertainties, and we observe values of χ^2 greater than 364 in more than 7% of the trials. In the final fit, all peaking-background parameters except the yields are fixed to the values extracted from the preliminary fit.

The final fit is performed as a scan over the values of the h_b peak position, with 39 steps in 1 MeV/c^2 intervals in the range $(9.880, 9.920)$ GeV/c^2 . At each step, a χ^2 fit is performed for the signal and background yields and the continuum background parameters. The fit procedure is validated with simulated experiments, and systematic uncertainties are evaluated for each point of the scan.

Figure 1 shows the m_R spectrum and the fit result. The nonpeaking background component dominates, with only the prominent $Y^{3\rightarrow 2}$ and $Y^{2\rightarrow 1}$ peaks clearly seen above this background. When comparing the fitted mass of the $Y^{3\rightarrow 2}$ peak with MC simulation, we observe a $+0.44 \pm 0.02(\text{stat.})$ MeV/c^2 displacement in data, which

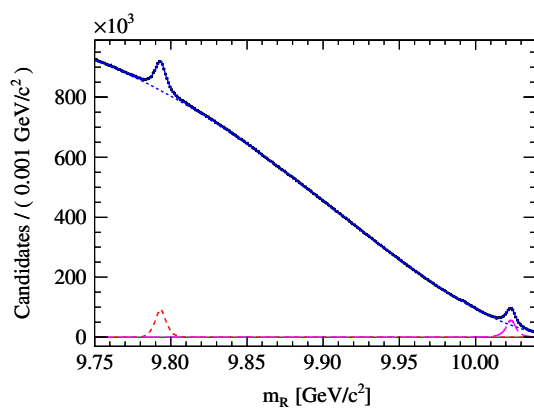


FIG. 1 (color online). The m_R spectrum: data (points) with the fitted model (solid line) superimposed. The short-dashed line is the contribution from the continuum component. Also shown are the $Y^{2\rightarrow 1}$ (dashed curve around 9.79 GeV/c^2) and $Y^{3\rightarrow 2}$ (long-dashed curve around 10.02 GeV/c^2) components. The h_b signal component is excluded from the superimposed model.

corresponds to a difference of $331.50 \pm 0.02(\text{stat.}) \pm 0.13(\text{syst.})$ MeV/c^2 between the $Y(3S)$ and $Y(2S)$ masses. The systematic uncertainty is dominated by uncertainties in the line shape and in the track momentum measurement. Details of the latter may be found in Ref. [21]. Other sources of uncertainty have been investigated and found to be of minor significance. These include the fit bias, the c.m. boost relative to the laboratory, the background model, and the PDF parameters. The position of the $Y^{2\rightarrow 1}$ peak is shifted by $+1.23 \pm 0.02(\text{stat.})$ MeV/c^2 in data with respect to simulation and corresponds to a difference of $561.7 \pm 0.0(\text{stat.}) \pm 1.2(\text{syst.})$ MeV/c^2 between the $Y(2S)$ and $Y(1S)$ masses, where the dominant sources of systematic uncertainty are the $Y(2S)$ momentum in the c.m. frame and the line shape model. Figure 2 shows the distribution of m_R after subtraction of the nonpeaking background. An expanded view of the $\chi_b^{J',J}$ region is presented in Fig. 3.

The inset of Fig. 2 shows an expanded view of the h_b signal region. The significance of a signal is evaluated at each point of the scan using the ratio, N/σ_N , of the signal yield N over its uncertainty σ_N . The largest enhancement over background is a 2.2 standard deviation (σ) excess (statistical only) at $m(h_b) \approx 9.916$ GeV/c^2 . Therefore, we do not obtain evidence for an h_b signal. The fitted h_b signal yield for $m(h_b) = 9.900$ GeV/c^2 is $[-1.1 \pm 2.4(\text{stat.})] \times 10^3$ events. Results for the $Y^{3\rightarrow 2}$, $Y^{2\rightarrow 1}$, $\chi_b^{1\rightarrow 1}$, and $\chi_b^{2\rightarrow 2}$ product branching fractions are presented in Table I.

In the following, reported quantities refer to $m(h_b) = 9.900$ GeV/c^2 . The ranges spanned by varying $m(h_b)$ in the interval $[9.880, 9.920]$ GeV/c^2 are given in parentheses. The following systematic uncertainties are associated with the signal yields. We observe a 10% discrepancy

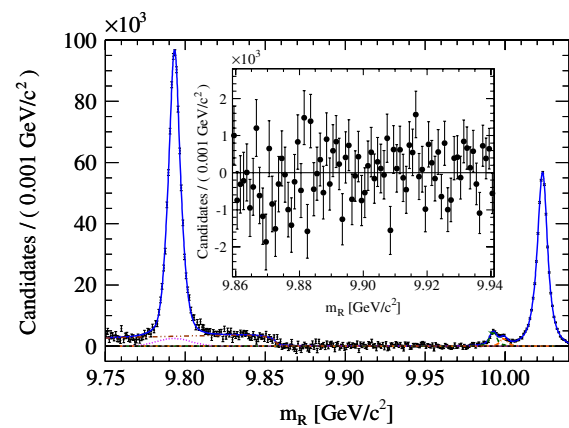


FIG. 2 (color online). The m_R spectrum after subtraction of the continuum background. The curves represent the fitted model (solid), the $Y_{\text{ISR}}^{2\rightarrow 1}$ (dotted), K_S^0 (double-dot-dashed), $\chi_b^{1,1}$ (dashed), and $\chi_b^{2,2}$ (dash-dotted) components. Inset: expanded view in the h_b region after subtraction of continuum and peaking backgrounds.

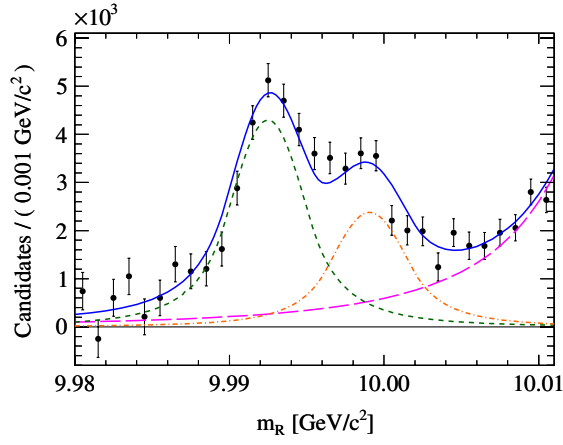


FIG. 3 (color online). The m_R spectrum in the $\chi_b^{J',J}$ region after subtraction of continuum and K_S^0 background components: points represent data, while the curves represent the fitted model (solid), the $\chi_b^{1,1}$ (dashed), $\chi_b^{2,2}$ (dash-dotted), and $Y^{3\rightarrow 2}$ (long-dashed) components.

between the m_R resolution values in data and MC for the $Y^{3\rightarrow 2}$ component, and translate this into an uncertainty of 0.1×10^3 (0.0×10^3 to 0.4×10^3) events on the h_b signal yield. A systematic uncertainty of 0.4×10^3 (0.3×10^3 to 0.5×10^3) events is estimated by varying the PDF parameters fixed in the fit by $\pm 1\sigma$, varying the overall width of the h_b PDF by 10%, setting the yield of the ISR $Y(2S)$ component to $\pm 1\sigma$ of the nominal value, and varying the K_S^0 component normalization and parameters within their uncertainties. Uncertainties related to the continuum background model amount to 0.2×10^3 (0.0×10^3 to 0.7×10^3) events. The additive systematic uncertainties on the yields of the $Y^{3\rightarrow 2}$, $\chi_b^{1\rightarrow 1}$, and $\chi_b^{2\rightarrow 2}$ components also account for the modeling of the $Y^{3\rightarrow 2}$ tails and for the assumption that the contributions of the $Y(3S) \rightarrow X\chi_{bJ'}(2P)$, $\chi_{bJ'}(2P) \rightarrow \pi^+\pi^-\chi_{bJ}$ decay chains with $J' \neq J$ or $J = 0$ are negligible [14,15].

The fit bias on the extracted yields, due to the choice of the fit model, is estimated with pseudoexperiments based on fully simulated Monte Carlo samples. We estimate a fit bias on the h_b signal yield of -2.8×10^3 (-3.0×10^3

to $+0.4 \times 10^3$) events. Fit biases for the other dipion transitions are listed in Table I. We do not correct the signal yields but rather assign the bias as a systematic uncertainty.

The following systematic uncertainties are associated with the reconstruction efficiency ϵ . The uncertainty due to the track-reconstruction efficiency is 3%. To assess the impact of data-MC differences on the $\pi^+\pi^-$ candidate selection efficiencies, we compare the relative variations of the $Y^{3\rightarrow 2}$ yield in data and MC when excluding selection requirements one at a time, and assign the full observed discrepancy to the systematic uncertainty. A total uncertainty of 2.3% in ϵ is obtained, including the statistical uncertainty (0.6%) in the $Y^{3\rightarrow 2}$ yield. The uncertainty in the number of $Y(3S)$ events is 1.1%. The above multiplicative systematic uncertainties affect the product branching fractions of all dipion transitions studied in this analysis. Differences in the selection efficiencies resulting from different angular distributions of the h_b decay products and different h_b hadronization models in the MC simulation contribute a 5% uncertainty. Model uncertainties in the simulation of the dipion kinematics, bottomonium hadronization, and $Y(2S)$ production channel (where applicable) in the $Y^{2\rightarrow 1}$, $Y^{3\rightarrow 2}$ [22], $\chi_b^{1\rightarrow 1}$, and $\chi_b^{2\rightarrow 2}$ decay chains result in systematic uncertainties on the efficiency of 1.3%, 0.5%, 0.6%, and 0.6%, respectively.

Product branching fractions are calculated by dividing the fitted yield by the efficiency and the number of $Y(3S)$ events, and are summarized in Table I. For $m(h_b) = 9.900 \text{ GeV}/c^2$ we find the branching fraction $\mathcal{B}_Y \equiv \mathcal{B}[Y(3S) \rightarrow \pi^+\pi^-h_b] = (-0.2 \pm 0.5 \pm 0.6) \times 10^{-4}$, where the first uncertainty is statistical and the second systematic, and set an upper limit (UL) $\mathcal{B}_Y < 1.2 \times 10^{-4}$ at 90% CL. The UL is calculated assuming a Gaussian sampling distribution $f(\mathcal{B}_Y)$ for \mathcal{B}_Y , which accounts for statistical and systematic uncertainties, and determining the value of UL for which $\int_0^{\text{UL}} f(\mathcal{B}_Y) d\mathcal{B}_Y = 0.9 \times \int_0^\infty f(\mathcal{B}_Y) d\mathcal{B}_Y$. Figure 4 reports the branching fractions \mathcal{B}_Y and the 90% CL ULs as a function of the assumed h_b mass. The branching fractions of the $\chi_{b1}(2P) \rightarrow \pi^+\pi^-\chi_{b1}$ and $\chi_{b2}(2P) \rightarrow \pi^+\pi^-\chi_{b2}$ transitions, given in Table I, are derived by correcting for

TABLE I. Summary of results for the signal yields, reconstruction efficiency ϵ , uncertainties on the branching fraction due to fit bias, systematic uncertainties on yields and efficiencies, the product branching fraction, and the branching fraction for the dipion transition.

	$h_b[m(h_b) = 9.900 \text{ GeV}/c^2]$	$\chi_b^{1\rightarrow 1}$	$\chi_b^{2\rightarrow 2}$	$Y^{3\rightarrow 2}$	$Y^{2\rightarrow 1}$
Yield	-1106 ± 2432	$31\,418 \pm 1851$	$17\,385 \pm 1456$	$543\,839 \pm 2928$	$906\,059 \pm 7407$
ϵ (%)	41.8	25.0	25.0	16.7	47.2
Fit bias (10^{-3})	-0.06	-0.09	-0.04	+0.2	+0.8
Yield error (10^{-3})	0.01	0.06	0.06	0.6	0.4
ϵ error (10^{-3})	0.00	0.05	0.03	1.3	0.8
$\prod \mathcal{B}$ (10^{-3})	...	$1.16 \pm 0.07 \pm 0.12$	$0.64 \pm 0.05 \pm 0.08$...	$17.8 \pm 0.2 \pm 1.1$
\mathcal{B} (10^{-3})	$-0.02 \pm 0.05 \pm 0.06$	$9.2 \pm 0.6 \pm 0.9$	$4.9 \pm 0.4 \pm 0.6$	$30.0 \pm 0.2 \pm 1.4$...

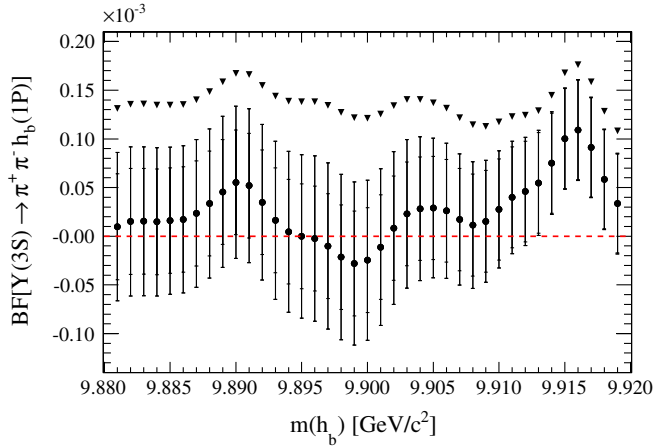


FIG. 4 (color online). Results for the $Y(3S) \rightarrow \pi^+ \pi^- h_b$ branching fraction (points with statistical and systematic uncertainties) as a function of the assumed h_b mass. The triangles indicate the upper limits at 90% CL.

the branching fractions of the $Y(3S) \rightarrow \gamma \chi_{b1}(2P)$ and $Y(3S) \rightarrow \gamma \chi_{b2}(2P)$ decays [4,23], respectively. The extracted values are in reasonable agreement with those found in the study by the CLEO Collaboration [4,15], where the two transitions could not be separated experimentally.

In summary, we present an inclusive analysis of the $\pi^+ \pi^-$ recoil mass spectrum in $Y(3S)$ decays. We measure the branching fraction

$$\begin{aligned} \mathcal{B}[Y(3S) \rightarrow \pi^+ \pi^- Y(2S)] \\ = (3.00 \pm 0.02(\text{stat.}) \pm 0.14(\text{syst.}))\%. \end{aligned}$$

This value is in reasonable agreement with, and more precise than, the current world average (2.45 ± 0.23)% [4].

The measured $Y(3S) - Y(2S)$ mass difference is $331.50 \pm 0.02(\text{stat.}) \pm 0.13(\text{syst.}) \text{ MeV}/c^2$.

We extract the product branching fractions

$$\begin{aligned} \mathcal{B}[Y(3S) \rightarrow X \chi_{b1}(2P)] \times \mathcal{B}[\chi_{b1}(2P) \rightarrow \pi^+ \pi^- \chi_{b1}] \\ = (1.16 \pm 0.07 \pm 0.12) \times 10^{-3}, \end{aligned}$$

$$\begin{aligned} \mathcal{B}[Y(3S) \rightarrow X \chi_{b2}(2P)] \times \mathcal{B}[\chi_{b2}(2P) \rightarrow \pi^+ \pi^- \chi_{b2}] \\ = (0.64 \pm 0.05 \pm 0.08) \times 10^{-3}, \quad \text{and} \end{aligned}$$

$$\begin{aligned} \mathcal{B}[Y(3S) \rightarrow XY(2S)] \times \mathcal{B}[Y(2S) \rightarrow \pi^+ \pi^- Y] \\ = (1.78 \pm 0.02 \pm 0.11)\%. \end{aligned}$$

A search for the h_b state, the 1P_1 state of bottomonium, in $Y(3S) \rightarrow \pi^+ \pi^- h_b$ decays does not provide evidence for this decay mode, and assuming the h_b mass to be $9.900 \text{ GeV}/c^2$, we set a 90% CL upper limit $\mathcal{B}_Y < 1.2 \times 10^{-4}$. We exclude, at 90% CL, values of \mathcal{B}_Y above 1.8×10^{-4} for a wide range of assumed h_b mass values. These results disfavor the calculations of Refs. [9–11]. Similarly, a recent measurement of the $Y(1^3D_J) \rightarrow Y(1S) \pi^+ \pi^-$ branching fraction [24] disfavors the calculations of Refs. [10,11]. The predictions of Ref. [12] are at least 1 order of magnitude smaller and are not contradicted by our result.

We are grateful for the excellent luminosity and machine conditions provided by our PEP-II colleagues, and for the substantial dedicated effort from the computing organizations that support *BABAR*. The collaborating institutions wish to thank SLAC for its support and kind hospitality. This work is supported by DOE and NSF (USA), NSERC (Canada), CEA and CNRS-IN2P3 (France), BMBF and DFG (Germany), INFN (Italy), FOM (The Netherlands), NFR (Norway), MES (Russia), MEC (Spain), and STFC (United Kingdom). Individuals have received support from the Marie Curie EIF (European Union) and the A. P. Sloan Foundation.

-
- [1] N. Brambilla *et al.* (Quarkonium Working Group), Report No. CERN-2005-005; *Eur. Phys. J. C* **71**, 1534 (2011).
 - [2] J. L. Rosner *et al.* (CLEO Collaboration), *Phys. Rev. Lett.* **95**, 102003 (2005); S. Dobbs *et al.* (CLEO Collaboration), *Phys. Rev. Lett.* **101**, 182003 (2008).
 - [3] S. Godfrey, *J. Phys. Conf. Ser.* **9**, 123 (2005).
 - [4] K. Nakamura *et al.* (Particle Data Group), *J. Phys. G* **37**, 075021 (2010).
 - [5] S. Godfrey and J. L. Rosner, *Phys. Rev. D* **66**, 014012 (2002).
 - [6] I. C. Brock *et al.* (CLEO Collaboration), *Phys. Rev. D* **43**, 1448 (1991); F. Butler *et al.* (CLEO Collaboration), *Phys. Rev. D* **49**, 40 (1994).
 - [7] J. P. Lees *et al.* (*BABAR* Collaboration), arXiv:1102.4565.
 - [8] I. Adachi *et al.* (Belle Collaboration), arXiv:1103.3419.
 - [9] S. F. Tuan, *Mod. Phys. Lett. A* **7**, 3527 (1992); *Phys. Rev. D* **42**, 3207 (1990).
 - [10] Y.-P. Kuang, S. F. Tuan, and T. M. Yan, *Phys. Rev. D* **37**, 1210 (1988).
 - [11] Y.-P. Kuang and T. M. Yan, *Phys. Rev. D* **24**, 2874 (1981); **41**, 155 (1990).
 - [12] M. B. Voloshin, *Sov. J. Nucl. Phys.* **43**, 1011 (1986).
 - [13] B. Aubert *et al.* (*BABAR* Collaboration), *Nucl. Instrum. Methods Phys. Res., Sect. A* **479**, 1 (2002).
 - [14] Y.-P. Kuang, *Front. Phys. China* **1**, 19 (2006).
 - [15] C. Cawlfild *et al.* (CLEO Collaboration), *Phys. Rev. D* **73**, 012003 (2006).
 - [16] S. Agostinelli *et al.*, *Nucl. Instrum. Methods Phys. Res., Sect. A* **506**, 250 (2003).

- [17] D.J. Lange, *Nucl. Instrum. Methods Phys. Res., Sect. A* **462**, 152 (2001).
- [18] T. Sjöstrand, *Comput. Phys. Commun.* **82**, 74 (1994).
- [19] G.C. Fox and S. Wolfram, *Nucl. Phys.* **B149**, 413 (1979).
- [20] M.J. Oreglia, Report No. SLAC-236, 1980, Appendix D; J.E. Gaiser, Report No. SLAC-255, 1982, Appendix F.
- [21] B. Aubert *et al.* (BABAR Collaboration), *Phys. Rev. D* **80**, 092005 (2009).
- [22] D. Cronin-Hennessy *et al.* (CLEO Collaboration), *Phys. Rev. D* **76**, 072001 (2007).
- [23] M. Artuso *et al.* (CLEO Collaboration), *Phys. Rev. Lett.* **94**, 032001 (2005).
- [24] P. del Amo Sanchez *et al.* (BABAR Collaboration), *Phys. Rev. D* **82**, 111102 (2010).